

Dipole-moment-induced effect on contact electrification for triboelectric nanogenerators

Peng Bai^{1,2,§}, Guang Zhu^{1,§}, Yu Sheng Zhou^{1,§}, Sihong Wang¹, Jusheng Ma², Gong Zhang², and Zhong Lin Wang^{1,3} (✉)

¹ School of Materials Science and Engineering, Georgia Institute of Technology, Atlanta, Georgia 30332-0245, USA

² Department of Mechanical Engineering, Tsinghua University, Beijing 100084, China

³ Beijing Institute of Nanoenergy and Nanosystems, Chinese Academy of Sciences, Beijing, China

[§] Authors with equal contribution and order of authors determined by coin toss.

Received: 13 February 2014

Revised: 22 March 2014

Accepted: 27 March 2014

© Tsinghua University Press
and Springer-Verlag Berlin
Heidelberg 2014

KEYWORDS

triboelectric
nanogenerator,
modulation,
dipole moment

ABSTRACT

Triboelectric nanogenerators (TENGs) have been demonstrated as an effective way to harvest mechanical energy to drive small electronics. The density of triboelectric charges generated on contact surfaces between two distinct materials is a critical factor for dictating the output power. We demonstrate an approach to effectively tune the triboelectric properties of materials by taking advantage of the dipole moment in polarized polyvinylidene fluoride (PVDF), leading to substantial enhancement of the output power density of the TENG. The output voltage ranged from 72 V to 215 V under a constant contact force of 50 N. This work not only provides a new method of enhancing output power of TENGs, but also offers an insight into charge transfer in contact electrification by investigating dipole-moment-induced effects on the electrical output of TENGs.

1 Introduction

The triboelectric effect, manifest as a type of contact electrification, is a common phenomenon in which charges are transferred from one material to another upon contact [1–6]. Although the triboelectric effect is yet to be fully explored due to a limited understanding of the fundamental mechanism [7–10], various applications have been developed for purposes such as photocopying [11], electrophotography [12], self-assembling systems [13, 14], electrostatic separation

[15] and recently developed triboelectric nanogenerators (TENGs) [16–18]. A TENG relies on the coupling between the triboelectric effect and electrostatic induction to convert mechanical energy into electricity. A major factor determining the output power of TENGs is the density of triboelectric surface charges, which serves as a driving force for induced free electrons. Since it is generally believed that the charge transfer between two distinct materials originates from the difference in their ability to gain electrons, the density of surface charges is primarily determined

Address correspondence to zlwang@gatech.edu

by the intrinsic properties of specific materials, though external factors in the environment may have a minor effect. As a consequence, there is a lack of effective means to enhance the output power of TENGs by modifying the intrinsic properties of materials in charge transfer [19–27].

In this work, we investigated the effect of an intrinsic dipole moment on the electrical output of TENGs. Polarized polyvinylidene fluoride (PVDF) thin films were utilized in fabricating a TENG without extra processing steps. Compared to a TENG fabricated using nonpolarized PVDF thin films, the output voltage could be either enhanced to 240% or reduced to 70%, depending on the direction of polarization. It is proposed that the presence of bond charges generated by aligned dipoles can influence the potential energy on the surface of PVDF thin films. As a result, the potential energy difference between the polarized PVDF and aluminum is modified, which leads to tunable quantity of charge being transferred upon contact. This work presents an initial effort to adjust the electrical output of TENGs over a wide range through changing the intrinsic electrical properties of a material. By proposing a mechanism that involves polarization-induced surface potential modification, this work also offers a new insight into contact electrification, suggesting that charge transfer is likely to be subject to manipulation by surface potential engineering.

2 Results and discussion

As sketched in Fig. 1(a), the TENG has a double-layer structure. The first layer is a piece of aluminum foil with uniformly sized and distributed nanopores on the surface (Fig. 1(b)). Based on previous work, the nanopore-based modification will further increase the effective contact area, thus enhancing the electrical output of TENGs (see the Electronic Supplementary Material (ESM)). The second layer is a piece of PVDF thin film deposited with copper on one side as the back electrode. Acrylic sheets were used as substrates. The two substrates were connected through two arc-shaped polyimide films that are anchored at edges, maintaining a gap between the substrates. An as-fabricated TENG is presented in Fig. 1(c). Two

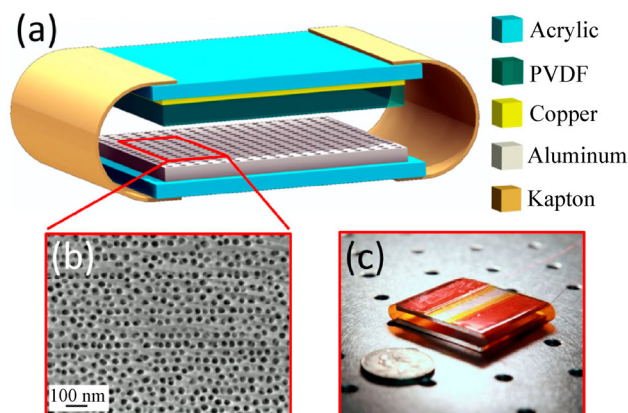


Figure 1 (a) Schematic of the TENG with a double-layer structure. (b) SEM image of nanopores on aluminum foil. (c) Photograph of a TENG.

categories of PVDF films were utilized, namely polarized films and nonpolarized films. Depending on the direction of the polarity, TENGs fabricated from polarized PVDF films are further categorized into two types. For clear reference, the ones with intrinsic dipole moment pointing to the back electrode are referred to as forward-polarized TENGs, while those with the opposite dipole moment are categorized as reverse-polarized TENGs (see the ESM). Further detailed fabrication specifications are discussed in the Experimental Section.

To characterize the electrical output, short-circuit current density (J_{sc}) and open-circuit voltage (V_{oc}) of TENGs fabricated using different types of PVDF films were measured under a periodic compressive force around 50 N applied by an electric shaker at a frequency of 4 Hz (Fig. S2 in the ESM). As shown in Fig. 2(a), a J_{sc} of $8.34 \mu\text{A}/\text{cm}^2$ was achieved by a forward-polarized TENG, corresponding to an increase of 36.3% when compared with a nonpolarized TENG that produces a J_{sc} of $6.13 \mu\text{A}/\text{cm}^2$. To further demonstrate the influence of dipole moment on the TENGs' output, J_{sc} of a reverse-polarized TENG was measured under the same conditions. A J_{sc} of $4.83 \mu\text{A}/\text{cm}^2$ was obtained, which is a decrease of about 21% in comparison to the nonpolarized TENG. Likewise, the obtained V_{oc} of the three types of TENGs shows similar results, as illustrated in Fig. 2(b). The largest V_{oc} of 215 V and smallest V_{oc} of 72 V correspond to the forward-polarized and reverse-polarized TENG, respectively. The differentiated electrical output from

the three categories of TENGs can be further evidenced by charge output, as shown in Fig. 2(c). Through a diode bridge, alternating electrons that flow between electrodes can be rectified, which leads to accumulative induced charges (accumulative Q). The forward-polarized TENG generates a charge output of $9.05 \mu\text{C}$ in 5 seconds, corresponding to induced charges of $0.51 \mu\text{C}$ per cycle. For the nonpolarized and reverse-polarized TENG, charges output reaches 4.72 and $2.50 \mu\text{C}$ in 5 seconds, in accordance to 0.25 and $0.14 \mu\text{C}$ per cycle, respectively. To eliminate random errors that may be caused by fabrication and measurement, five batches of devices were tested for each category of TENGs under the same conditions. As shown in Fig. 2(d), average J_{sc} values of $7.55 \mu\text{A}/\text{cm}^2$, $5.40 \mu\text{A}/\text{cm}^2$, and $4.28 \mu\text{A}/\text{cm}^2$ were obtained from

forward-polarized, nonpolarized, and reverse-polarized TENGs, respectively. The same trend also applies to the average amplitude of V_{oc} and equivalent direct current density (equivalent J_{sc}) which is defined as the average quantity of positive charges flowing through the circuit per second after being rectified (see the ESM), as shown in Figs. 2(e) and 2(f), respectively. Taking the average amplitude of V_{oc} for example, it shows over three-fold enhancement between the forward-polarized and reverse-polarized TENGs. Resistors were utilized as external loads to investigate the output power of different types of TENGs under a compressive force of around 50 N. As shown in Fig. 2(g), a peak power of 3.74 mW was achieved at a load resistance of $40 \text{ M}\Omega$ for the forward-polarized TENG, and a peak power of 1.19 mW was achieved

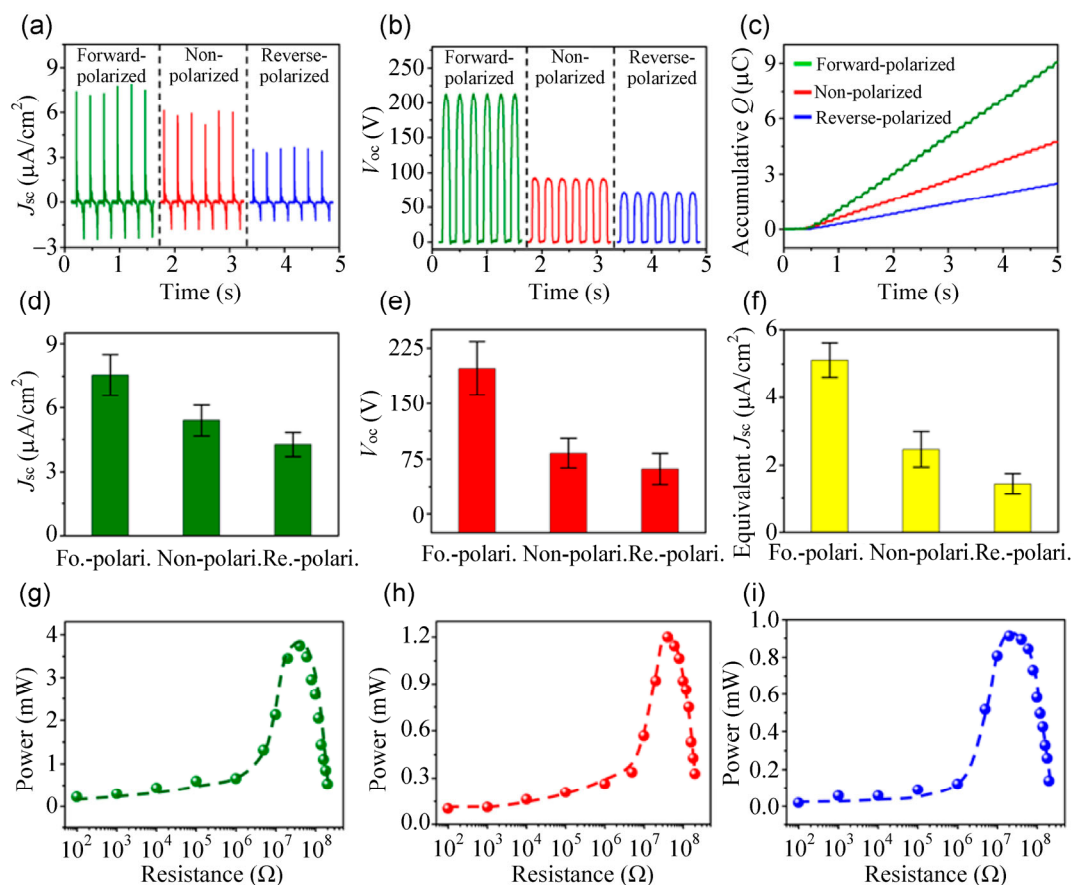


Figure 2 (a) J_{sc} of TENGs fabricated using different types of PVDF films under a periodic compressive force around 50 N applied by an electric shaker at a frequency of 4 Hz. (b) V_{oc} of TENGs fabricated using different types of PVDF films. (c) Accumulative Q generated by TENGs fabricated using different types of PVDF films. (d) Average J_{sc} of TENGs fabricated using different types of PVDF films. (e) Average V_{oc} of TENGs fabricated using different types of PVDF films. (f) Average equivalent J_{sc} of TENGs fabricated using different types of PVDF films. (g) Dependence of the peak power output of the forward-polarized TENG on the resistance of the external load. (h) Dependence of the peak power output of the nonpolarized TENG on the resistance of the external load. (i) Dependence of the peak power output of the reverse-polarized TENG on the resistance of the external load. The curve is a fitted result.

at 40 M Ω for the nonpolarized TENG (Fig. 2(h)) while a smaller peak power of 0.91 mW was achieved at 20 M Ω for the reverse-polarized TENG (Fig. 2(i)).

Though a variety of factors could have an influence on the electrical output of TENGs, considering the constancy of the other parameters—materials selection, fabrication process, device dimension, and measurement conditions—the differences in the electrical output of the three types of TENGs most likely originate from the variations in the surface charge density. Therefore, it is proposed that the intrinsic dipole moment alters the surface potential level of the PVDF film, thus modulating surface charge transfer between the PVDF and the aluminum electrode. Abundant experimental evidence has shown that charge transfer between metals and dielectrics occurs via tunneling, which results from unequal effective work functions (Φ) of two materials [1, 2, 28]. As illustrated by a simplified band diagram in Fig. 3(a), the surface energy state of nonpolarized PVDF can be represented by an characteristic energy level with an effective work function around 5.0 eV [29, 30], which is higher than that of aluminum (4.2 eV). As a consequence, when aluminum and PVDF are brought into contact, electrons tunnel from the Fermi level of aluminum (E_F) to the characteristic energy level of PVDF (E_0), making the PVDF surface negatively charged. The transfer of electrons continues until the two energy levels are lined up. Therefore, it is apparent that the density of surface charge is directly related to the potential difference between the two energy levels, which is primarily determined by materials' properties, such as chemical composition [1, 2, 31]. Depending on the relative magnitudes of E_F and E_0 , electrons tend to flow out of the filled Fermi level of aluminum into the empty surface states of the PVDF. The probability of charge transfer is a function of the potential difference between the two adjacent materials [32]. As shown in Fig. 3(b), the electric field developed by charge transfer raises the energy of the electrons in PVDF's surface states by $\delta E(Q)$ relative to E_F , and the potential difference between aluminum and PVDF consequently becomes smaller. When the quantity of charge reaches its saturation value, the transfer of charge will cease. The center of positive charges and the center of negative charges do not coincide in

every molecule of PVDF in its polar β -phase, but the bond charge is zero when the β -phase forms naturally because of the random arrangement of dipoles. After being polarized along the thickness, all the dipole moments are oriented along the same direction, resulting in bond charges on the surfaces of the PVDF thin film (see the ESM) [33–36]. Although molecules or space charges will be adsorbed onto the surfaces of PVDF, the bond charges cannot be always completely compensated, and partially compensated surfaces are likely to be the usual state in air [37–39]. If the film is forward-polarized with positive bond charges on the surface that is contact with the aluminum while the other side of its surface is covered by the back electrode, the characteristic energy level of PVDF will be reduced to E_0' on the surface as shown in Fig. 3(c). Such a shift of energy level leads to an enlarged potential difference with the Fermi level of aluminum, which will in turn increase the probability of charge transfer by tunneling upon contact. As a result, an enhanced density of surface triboelectric charge can be expected. In contrast, the negative bond charges on the surface of reverse-polarized PVDF will raise the characteristic energy level to E_0'' as shown in Fig. 3(d),

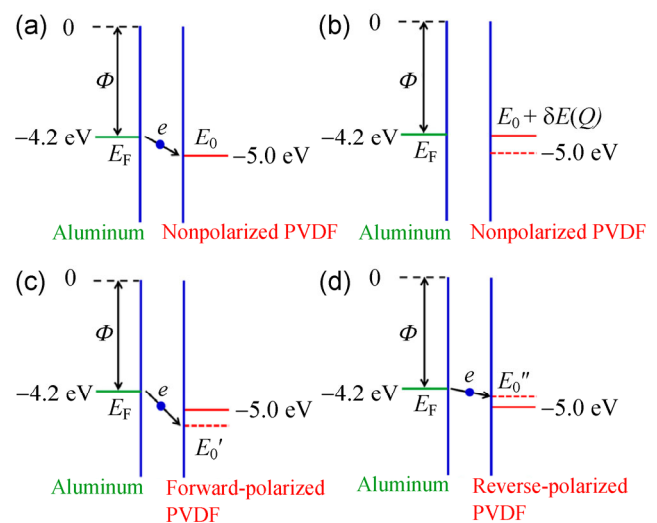


Figure 3 (a) Schematic energy band diagram illustrating the process when electrons tunnel between E_F and E_0 . (b) The electric field developed by charge transfer raises the energy of the electrons in the PVDF's surface states by $\delta E(Q)$. (c) The positive bond charges of the forward-polarized PVDF reduce the characteristic energy level of PVDF to E_0' . (d) The negative bond charges of the reverse-polarized PVDF increase the characteristic energy level of PVDF to E_0'' .

and thus reduce the density of triboelectric charge in comparison with the nonpolarized PVDF film. Based on previous studies, the surface triboelectric charges are the direct driving force for transport of induced electrons between electrodes in a TENG [18, 20]. The surface charge density thus determines the amount of induced electrons that flow to screen electric field from the triboelectric charges. Therefore, forward-polarized PVDF films afford enhanced electrical output, while reverse-polarized PVDF does the opposite. A detailed description of the electricity generation of a TENG is sketched in Fig. S6 (in the ESM).

To validate the above proposed mechanism, we further investigated the dependence of the equivalent J_{sc} from different types of TENGs on the interactive force during contact. As shown in Fig. 4(a), the enhanced equivalent J_{sc} from nonpolarized TENGs as a function of the contact force is attributed to the increased contact area between the PVDF and the aluminum, which has been discussed in previous reports [18, 26]. Also in accordance with literature, such dependence has a linear behavior in the range

of small contact force [20, 26]. It is noteworthy that the equivalent J_{sc} from TENGs based on forward-polarized PVDF presents an enhanced growth rate with a larger slope in Fig. 4(a). This is due to the increased surface charge density that results from the intrinsic dipole moment. It is to be noted that the effect of the dipole moment can play a role only when the two materials come into contact. As a result, such an effect can be assumed to be also linearly related to the contact force. Therefore, it is expected on the basis of our proposed mechanism that the ratio between the two types of TENGs remains at a constant value that is independent of the contact force. A detailed examination of the experimental data in Table S1 (in the ESM) confirms our hypothesis and thus validates the proposed mechanism. Likewise, the equivalent J_{sc} obtained from reverse-polarized TENGs also closely follows our expectation but shows the opposite effect from the intrinsic dipole moment. As shown in Fig. 4(b), to illustrate the different electrical output of different types of TENGs under the same conditions, we connected the TENGs and resistances as external loads

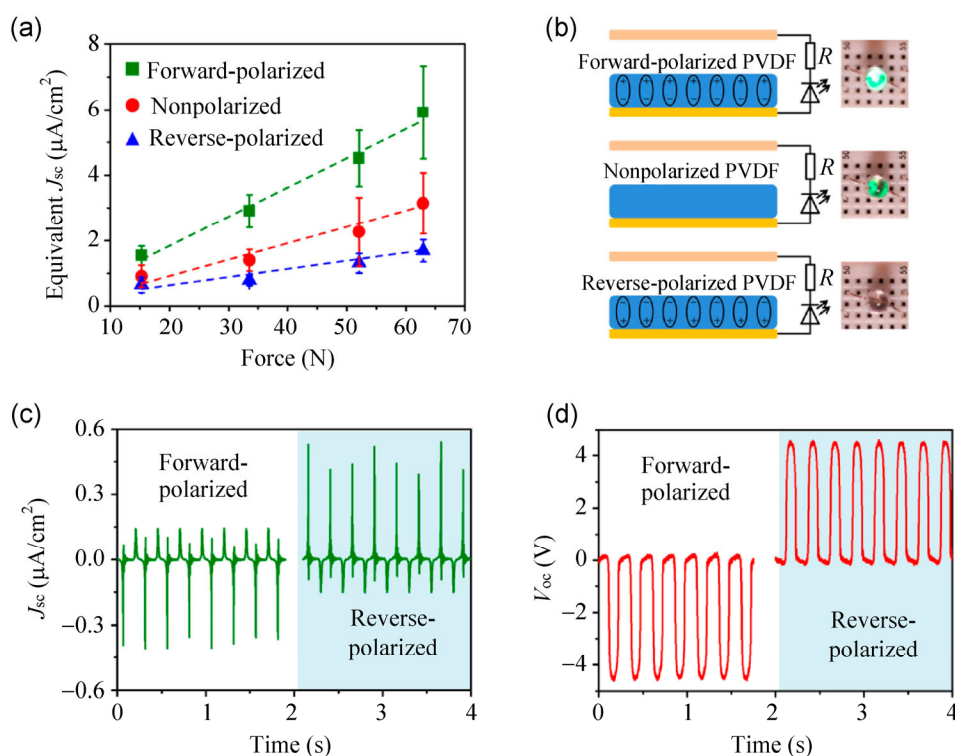


Figure 4 (a) Equivalent J_{sc} of TENGs fabricated using different types of PVDF under different contact force. Lines are the fitting results. (b) Circuit diagrams and the different performances among TENGs fabricated using different types of PVDF when they were used as direct power source for LED bulbs. (c) J_{sc} and (d) V_{oc} of piezoelectric output from PVDF thin films under a contact force of around 50 N.

in series to drive LED bulbs. TENGs worked under a contact force around 50 N, and the performance of each type of TENGs can be observed by the LED bulb. The LED bulb can be completely lit up when the forward-polarized TENG was used as the power source, while the LED bulb was comparatively less bright when we use the nonpolarized TENG as the power source. In addition, because of the minimum electrical output, reverse-polarized TENGs cannot even drive the LED bulb.

It is recognized that polarized PVDF is also known as a type of piezoelectric material that generates additional dipole moments along the poling direction in response to induced strain as a result of externally applied pressure [33]. The piezoelectric output of polarized PVDF thin films was measured independently under the same conditions as for the TENGs. A layer of copper was deposited on the back of the polarized PVDF thin films as a back electrode while a layer of aluminum was deposited as the other electrode. When a compressive force is applied onto the top of the aluminum electrode, a potential difference will be developed with the negative polarity at the aluminum side for the forward-polarized PVDF thin films and the positive one for the reverse-polarized PVDF thin films, resulting in a voltage signal (Fig. S7, in the ESM). The piezoelectric effect can be ruled out as a possible reason for the modified electrical output of the TENGs based on the following four reasons: (1) Both the short-circuit current density (Fig. 4(c)) and open-circuit voltage (Fig. 4(d)) from the piezoelectric signal are only about 10% of the triboelectric output under the same contact force of 50 N (a J_{sc} around $0.5 \mu\text{A}/\text{cm}^2$ and a V_{oc} around 4.5 V). Such a big difference in the magnitude of triboelectric and piezoelectric output means that the influence of piezoelectricity on the electrical output of TENGs is negligible. It needs to be noted that the polarity of piezoelectric output from forward-polarized PVDF thin films is opposite to that from the reverse-polarized PVDF thin films, which is because the directions of piezoelectric fields established in forward-polarized and reverse-polarized PVDF thin films are opposite to each other as we mentioned before; (2) for the forward-polarized TENG, the polarity of piezoelectric output is opposite to that of the triboelectric output. According to the electricity-

generation principle of TENGs, a positive electrical signal will be generated when a periodic compressive force is applied onto the top of the aluminum electrode for the forward-polarized TENG, but the corresponding piezoelectric output is negative as shown in Figs. 4(c) and 4(d). If the piezoelectric and triboelectric output can be added up, the electrical output of forward-polarized TENGs will be smaller than that of the reverse-polarized TENGs, which is not consistent with the experimental results. Therefore, the assumption of superposition between the piezoelectric output and triboelectric output does not hold; (3) the electrical output from the TENG and the piezoelectric effect are not synchronized processes. For the triboelectric output, the electrical signal can be only generated either when the two contacting materials approach or when they start to separate from each other. The TENG does not produce electricity when the two surfaces stay in contact, while piezoelectric effect becomes effective only when the contact is achieved with a pressure in between, which is consistent with the fact that the current signal of the triboelectric output lasts longer than the one of piezoelectric output (Fig. S8, in the ESM). Therefore, the triboelectric charge density that actually determines the electrical output of the TENG thus becomes independent of the piezoelectric effect; (4) we investigated the dependence of the electrical output on the contact force for all three types of TENGs (Fig. 4(a)). It was found that the ratio between the equivalent J_{sc} of forward-polarized TENGs and nonpolarized TENGs remains the same at different contact forces. Such a result can also be obtained for non-polarized TENGs and reverse-polarized TENGs. Given that the piezoelectric-induced dipole moment is force-dependent, if it plays a role in modifying the electrical output, the above-mentioned ratio would either increase or decrease due to the fact that a larger contact force results in a larger piezoelectric output. Therefore, it can be concluded that it is the intrinsic dipole moment rather than the piezoelectric effect that results in the change in electrical output.

3 Conclusions

We have investigated the effect of an intrinsic dipole moment on a TENG's electrical output. The electrical

output can be either enhanced or weakened by utilizing forward-polarized or reverse-polarized PVDF as the contact material due to the influence of intrinsic dipole moments on the characteristic potential energy on the surface of PVDF thin films. The output voltage ranged from 72 V to 215 V under a constant contact force around 50 N. This study demonstrates the possibility of adjusting the electrical output of TENGs over a wide range through changing the intrinsic properties of a material, and also offers a new insight into contact electrification.

4 Experimental section

4.1 Fabrication of a TENG with PVDF film as the contact material

Two pieces of cast acrylic glass were prepared as substrates (3.8 cm × 3.8 cm × 0.6 cm), and Kapton films with a thickness of 125 μm were used as spacers. Nonpolarized or polarized PVDF thin films (Piezotech S.A.S, France) with a thickness of 25 μm were deposited with 100 nm of copper by magnetron sputtering and were adhered on a substrate with the uncoated side exposed. Subsequently, a piece of aluminum foil with nanopore-based modification (3.8 cm × 3.8 cm × 125 μm) was adhered onto the substrate at the corresponding position. Finally, conducting wires were connected to the two metal layers as lead wires for electrical measurements.

4.2 Nanopore-based surface modification

Electrochemical anodization was applied to the aluminum foil in 3% (mass fraction) oxalic acid (H₂C₂O₄) electrolyte. A platinum plate was used as the cathode. The aluminum foil was anodized under a bias voltage of 30 V for 5 hours. The alumina layer was etched away in a solution of 20 g/L chromic acid at 60 °C for 2 h. Then the aluminum foil was rinsed with deionized water and dried in air.

Acknowledgements

This research was supported by U.S. Department of Energy, Office of Basic Energy Sciences (Award

DE-FG02-07ER46394), NSF (0946418), the Knowledge Innovation Program of the Chinese Academy of Sciences (Grant No. KJ CX2-YW-M13), and the “Thousands Talents” program for Pioneer Researchers and their Innovation Team. The authors thank Qingshen Jing and Jun Chen for technical assistance. Peng Bai thanks the Chinese Scholarship Council for support. Patents have been filed based on the research results presented in this manuscript.

Electronic Supplementary Material: Supplementary material (illustration of the force-dependent contact area, measurement of the contact force, properties and structure of β-PVDF, dipole moments in the β-phase of PVDF before and after polarization, definition of equivalent direct current, enlarged view of J_{scr} a detailed description of the electricity generation of a TENG, electricity generation process by the piezoelectric effect with polarized PVDF thin films in open-circuit conditions, enlarged view of electrical signals from the triboelectric output and the piezoelectric output, equivalent J_{sc} from different types of TENGs under different contact forces, and technical datasheet for the polarized PVDF film) is available in the online version of this article at <http://dx.doi.org/10.1007/s12274-014-0461-8>.

References

- [1] Lowell, J.; Rose-Innes, A. C. Contact electrification. *Adv. Phys.* **1980**, *29*, 947–1023.
- [2] Harper, W. R. *Contact and Frictional Electrification*; Laplacian Press: Morgan Hill, 1998.
- [3] Horn, R. G.; Smith, D. T. Contact electrification and adhesion between dissimilar material. *Science* **1992**, *256*, 362–364.
- [4] Horn, R. G.; Smith, D. T.; Grabbe, A. Contact electrification induced by monolayer modification of a surface and relation to acid–base interactions. *Nature* **1993**, *366*, 442–443.
- [5] Pai, D. M.; Springett, B. E. Physics of electrophotography. *Rev. Mod. Phys.* **1993**, *65*, 163–211.
- [6] Liu, C.-Y.; Bard, A. J. Electrostatic electrochemistry at insulators. *Nat. Mater.* **2008**, *7*, 505–509.
- [7] Gibson, H. W. Control of electrical properties of polymers by chemical modification. *Polymer* **1984**, *25*, 3–27.
- [8] McCarty, L. S.; Whitesides, G. M. Electrostatic charging due to separation of ions at interfaces: Contact electrification of ionic electrets. *Angew. Chem. Int. Ed.* **2008**, *47*, 2188–2207.

- [9] Davies, D. K. Charge generation on dielectric surfaces. *J. Phys. D: Appl. Phys.* **1969**, *2*, 1533.
- [10] Diaz, A. F.; Guay, J. Contact charging of organic materials: Ion vs. electron transfer. *IBM J. Res. Dev.* **1993**, *37*, 249–260.
- [11] Schein, L. B. *Electrophotography and Development Physics*; Laplacian: Morgan Hill, 1996.
- [12] Burland, D. M.; Schein, L. B. Physics of electrophotography. *Phys. Today* **1986**, *39*, 46–53.
- [13] Grzybowski, B. A.; Winkleman, A.; Wiles, J. A.; Brumer, Y.; Whitesides, G. M. Electrostatic self-assembly of macroscopic crystals using contact electrification. *Nat. Mater* **2003**, *2*, 241–245.
- [14] Grzybowski, B. A.; Wiles, J. A.; Whitesides, G. M. Dynamics self-assembly of rings of charged metallic spheres. *Phys. Rev. Lett.* **2003**, *90*, 083903.
- [15] Kwetkus, B. A. Particle triboelectrification and its use in the electrostatic separation process. *Part. Sci. Technol.* **1998**, *16*, 55–68.
- [16] Fan, F.-R.; Lin, L.; Zhu, G.; Wu, W. Z.; Zhang, R.; Wang, Z. L. Transparent triboelectric nanogenerators and self-powered pressure sensors based on micropatterned plastic films. *Nano Lett.* **2012**, *12*, 3109–3114.
- [17] Zhu, G.; Pan, C. F.; Guo, W. X.; Chen, C.-Y.; Zhou, Y. S.; Yu, R. M.; Wang, Z. L. Triboelectric-generator-driven pulse electrodeposition for micropatterning. *Nano Lett.* **2012**, *12*, 4960–4965.
- [18] Wang, S. H.; Lin, L.; Wang, Z. L. Nanoscale triboelectric-effect-enabled energy conversion for sustainably powering portable electronics. *Nano Lett.* **2012**, *12*, 6339–6346.
- [19] Zhu, G.; Lin, Z.-H.; Jing, Q. S.; Bai, P.; Pan, C. F.; Yang, Y.; Zhou, Y. S.; Wang, Z. L. Toward large-scale energy harvesting by a nanoparticle-enhanced triboelectric nanogenerator. *Nano Lett.* **2013**, *13*, 847–853.
- [20] Xie, Y. N.; Wang, S. H.; Lin, L.; Jing, Q. S.; Lin, Z.-H.; Niu, S. M.; Wu, Z. Y.; Wang, Z. L. Rotary triboelectric nanogenerator based on a hybridized mechanism for harvesting wind energy. *ACS Nano* **2013**, *7*, 7119–7125.
- [21] Bai, P.; Zhu, G.; Liu, Y.; Chen, J.; Jing, Q. S.; Yang, W. Q.; Ma, J. S.; Zhang, G.; Wang, Z. L. Cylindrical rotating triboelectric nanogenerator. *ACS Nano* **2013**, *7*, 6361–6366.
- [22] Lin, L.; Wang, S. H.; Xie, Y. N.; Jing, Q. S.; Niu, S. M.; Hu, Y. F.; Wang, Z. L. Segmentally structured disk triboelectric nanogenerator for harvesting rotational mechanical energy. *Nano Lett.* **2013**, *13*, 2916–2923.
- [23] Yang, X. H.; Zhu, G.; Wang, S. H.; Zhang, R.; Lin, L.; Wu, W. Z.; Wang, Z. L. A Self-powered electrochromic device driven by a nanogenerator. *Energ. Environ. Sci.* **2012**, *5*, 9462–9466.
- [24] Lin, Z.-H.; Zhu, G.; Zhou, Y. S.; Yang, Y.; Bai, P.; Chen, J.; Wang, Z. L. A Self-powered triboelectric nanosensor for mercury ion detection. *Angew. Chem. Int. Ed.* **2013**, *52*, 5065–5069.
- [25] Bai, P.; Zhu, G.; Lin, Z.-H.; Jing, Q. S.; Chen, J.; Zhang, G.; Ma, J. S.; Wang, Z. L. Integrated multilayered triboelectric nanogenerator for harvesting biomechanical energy from human motion. *ACS Nano* **2013**, *7*, 3713–3719.
- [26] Yang, Y.; Zhang, H. L.; Lee, S.; Kim, D.; Hwang, W.; Wang, Z. L. Hybrid energy cell for degradation of methyl orange by self-powered electrocatalytic oxidation. *Nano Lett.* **2013**, *13*, 803–808.
- [27] Kim, H.; Kim, S. M.; Son, H.; Kim, H.; Park, B.; Ku, J.; Sohn, J. I.; Im, K.; Jang, J. E.; Park, J.-J.; et al. Enhancement of piezoelectricity via electrostatic effects on a textile platform. *Energ. Environ. Sci.* **2012**, *5*, 8932–8936.
- [28] Harper, W. R. The Volta effect as a cause of static electrification. *Proc. R. Soc. Lond. A* **1951**, *205*, 83–103.
- [29] Lowell, J. Tunnelling between metals and insulators and its role in contact electrification. *J. Phys. D: Appl. Phys.* **1979**, *12*, 1541.
- [30] Davies, D. K. Charge generation on dielectric surfaces. *J. Phys. D: Appl. Phys.* **1969**, *2*, 1533.
- [31] Lowell, J. The electrification of polymers by metals. *J. Phys. D: Appl. Phys.* **1976**, *9*, 1571.
- [32] Grzybowski, B. A.; Fialkowski, M.; Wiles, J. A. Kinetics of contact electrification between metals and polymers. *J. Phys. Chem. B* **2005**, *109*, 20511–20515.
- [33] Xue, X. Y.; Wang, S. H.; Guo, W. X.; Zhang, Y.; Wang, Z. L. Hybridizing energy conversion and storage in a mechanical-to-electrochemical process for self-charging power cell. *Nano Lett.* **2012**, *12*, 5048–5054.
- [34] Lefki, K.; Dormans, G. J. M. Measurement of piezoelectric coefficients of ferroelectric thin films. *J. Appl. Phys.* **1994**, *76*, 1764.
- [35] Kalinin, S. V.; Bonnell, D. A. Local potential and polarization screening on ferroelectric surfaces. *Phys. Rev. B* **2001**, *63*, 125411.
- [36] Womes, M.; Bihler, E.; Eisenmenger, W. Dynamics of polarization growth and reversal in PVDF Films. *IEEE Trans. Electr. Ins.* **1989**, *24*, 461–468.
- [37] Palto, S.; Blinov, L.; Dubovik, E.; Fridkin, V.; Petukhova, N.; Sorokin, A.; Verkhovskaya, K.; Yudin, S. Ferroelectric Langmuir–Blodgett films. *Ferroelectr. Lett.* **1995**, *19*, 65–68.
- [38] Saurenbach, F.; Terris, B. D. Imaging of ferroelectric domain walls by force microscopy. *Appl. Phys. Lett.* **1990**, *56*, 1703.
- [39] Hong, J. W.; Park, S.-I.; Khim, Z. G. Measurement of hardness, surface potential, and charge distribution with dynamic contact mode electrostatic force microscope. *Rev. Sci. Instrum.* **1999**, *70*, 1735.